The multi-modality neuroimaging analysis identified an essential genetic variant associated with Parkinson's disease

Zhichun Chen[1,2], Bin Wu[3], Guanglu Li[1], Liche Zhou[1], Lina Zhang[4], Jun Liu[1,*]

[1]Department of Neurology and Institute of Neurology, Ruijin Hospital affiliated to Shanghai Jiao Tong University School of Medicine, Shanghai, 200025, China;

[2]Department of Neurology, The Second Xiangya Hospital, Central South University, 139 Renminzhong Road, Changsha, 410011, China;

[3]Department of Neurology, Xuchang Central Hospital affiliated with Henan University of Science and Technology, Henan, 461000, China;

[4]Department of Biostatistics, Shanghai Jiao Tong University School of Medicine, Shanghai, 200025, China.

[*]**For correspondence:** jly0520@hotmail.com

Keywords: Parkinson's disease; genetic variant; brain networks; graphical analysis; *GPNMB*.

Character in the title: 116

Number of words in Abstract: 191

Number of words in the body: 8485

Total figures:5

Total Table supplements:2

Total Figure supplements: 4

Abstract

Over 90 genetic variants have been found to be associated with Parkinson's disease (PD) in genome-wide association studies, however, the neural mechanisms of these identified genetic variants conferring risk of PD were largely unexplored. The objective of this study was to identify essential genetic variants in PD for future functional and mechanistic studies. We revealed 14 single nucleotide polymorphisms (SNPs) conferring risk of PD were significantly correlated with brain gene expressions. Although they were not significantly associated with the clinical presentations of PD patients in multivariate regression models, multi-SNP models constructed by several genetic variants powerfully predicted clinical presentations of PD patients. Among 14 SNPs, *GPNMB* rs199347 significantly modified the activity of sensorimotor network (adjusted $p < 0.0007$, FDR corrected) after adjusting age, sex, disease duration, and the genotypes of remaining 13 SNPs. Graph-based network analysis further demonstrated that *GPNMB* rs199347 had remarkable effects on the global topology of functional network and specifically shaped the nodal network metrics of bilateral caudate. *GPNMB* rs199347 was not associated with significant changes of structural network metrics. Our findings support that *GPNMB* rs199347 is an essential genetic variant specifically shaping functional network of PD patients.

Introduction

Parkinson's disease (PD) is the most common movement disorder and the second most common neurodegenerative disease in the world. Since PD was first reported in 1817, the study of PD has a history of more than 200 years. However, PD patients remain still incurable now due to less understanding of PD pathogenesis. Recent studies have shown that genetic variation is a fundamental mechanism to drive the initiation and progression of PD (Bingol et al., 2014; Burmann et al., 2020; Dunn, O'Connell, & Kaczorowski, 2019; Manzanillo et al., 2013; Matheoud et al., 2019; Matheoud et al., 2016; Sliter et al., 2018; van Veen et al., 2020; Wie et al., 2021). Additionally, a rapidly growing number of genes associated with PD risk have been detected, including *GPNMB* and *MAPT* (Chang et al., 2017; Diaz-Ortiz et al., 2022; Nalls et al., 2019). However, the specific roles of previously identified risk genes in PD pathogenesis remain unclear. With the discovery of new risk genes in PD, in recent years, deciphering the biological functions of PD-associated genes and their roles in the occurrence and progression of PD from the molecular, cellular, neural circuit, and behavior levels has continuously driven the new research breakthroughs in PD (Bingol et al., 2014; Burmann et al., 2020; Manzanillo

et al., 2013; Matheoud et al., 2019; Matheoud et al., 2016; Sliter et al., 2018; van Veen et al., 2020; Wie et al., 2021). Over the past decade, both the physiological and pathological functions of a range of PD-associated genes have been dissected, including *SNCA* (Burmann et al., 2020; Fusco et al., 2017; Peng et al., 2018; Shahnawaz et al., 2020), *Parkin* (Bingol et al., 2014; Manzanillo et al., 2013; Matheoud et al., 2016; Sliter et al., 2018), *PINK1* (Matheoud et al., 2019; Matheoud et al., 2016; Sliter et al., 2018), *LRRK2* (Cookson, 2010; Deniston et al., 2020; Liu et al., 2018; Nguyen et al., 2011; Simuni et al., 2020; Watanabe et al., 2020), *TMEM175* (Wie et al., 2021), and *ATP13A2* (van Veen et al., 2020). These breakthroughs deepen our understanding of the neurodegenerative process of PD and lay the foundation for the exploration of new therapeutic targets.

Currently, one of our main challenges is to investigate the biological functions and pathogenic or protective roles of numerous single nucleotide polymorphisms (SNPs) that have been identified in PD. However, it is time-consuming and laborious to study the biological functions and its specific roles in disease pathogenesis for each PD-associated SNP. Therefore, we can set some criteria at different levels (ie. molecular or network) to screen out those SNPs that deserve further exploration. Previously, several SNPs have been reported to modify clinical features of PD patients, including motor symptoms, non-motor symptoms, striatal dopamine transporter (DAT) uptake, and biomarkers in cerebrospinal fluid (CSF) (Backstrom et al., 2018; Bekris et al., 2015; Corvol et al., 2011; Davis et al., 2016; Latourelle et al., 2017; Mata et al., 2014; Nalls et al., 2019; Nishioka et al., 2006; Simuni et al., 2020; Webb & Willette, 2017). Through expression quantitative trait loci (eQTL) analysis, studies have also reported some SNPs conferring risk of PD were associated with brain gene expressions (Chang et al., 2017; Jiang et al., 2020; Murthy et al., 2017; Pierce & Coetzee, 2017). Therefore, those SNPs significantly associated with clinical features and brain gene expressions are more likely to be functional genetic variants in PD.

Over the past three decades, the methodologies of functional magnetic resonance imaging (fMRI) have been utilized to identify the structural or functional presentations associated with specific genetic variants (Glahn, Thompson, & Blangero, 2007; Hernandez et al., 2017; Mascheretti et al., 2017). Furthermore, recent studies have combined the functional and structural network analysis to identify network alterations associated with genetic variants and clinical features of diseases (Filippi et al., 2020; Fishman, Datko, Cabrera, Carper, & Muller, 2015; Hong, Bernhardt, Gill, Bernasconi, & Bernasconi, 2017; Imperiale et al., 2018).

Therefore, multi-modality neuroimaging analysis is a useful approach to examine whether a SNP is a functional genetic variant in PD. In this study, we combined eQTL data, clinical phenotype association analysis, and neuroimaging analysis to identify important functional genetic variants in PD based on Parkinson's Progression Markers Initiative (PPMI) database (www.ppmi-info.org/data).

Results

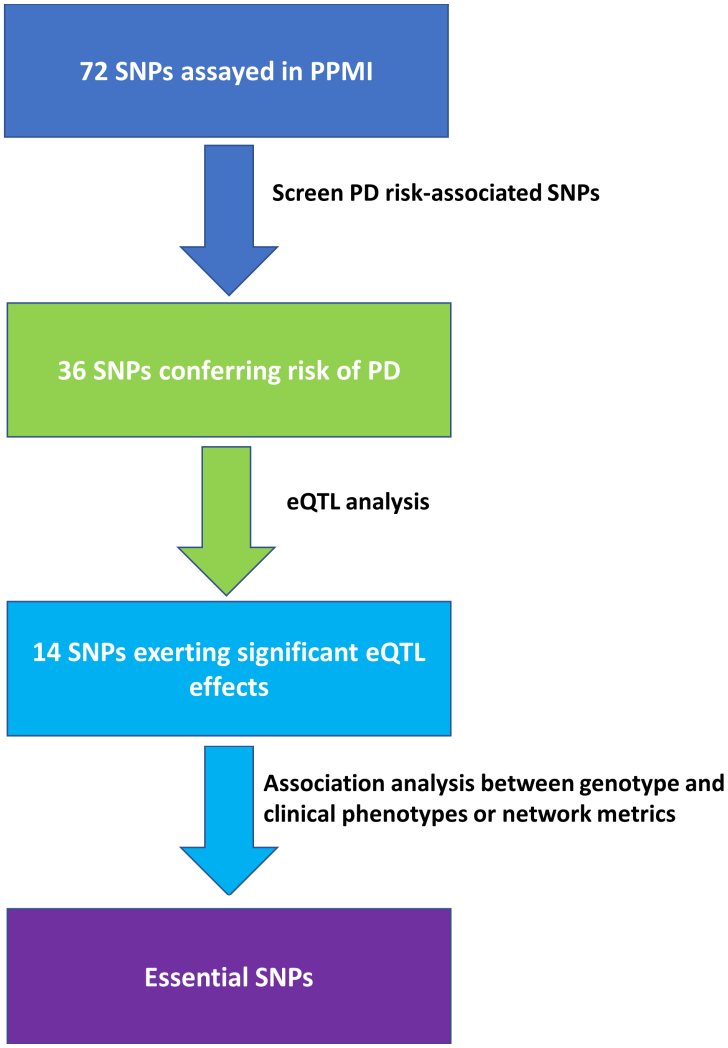

Figure 1. The screening process of essential genetic variants from 72 SNPs assayed in PPMI database.

Demographical variables

The clinical data of 198 PD patients and 189 control participants were shown and compared in **Table supplement 1**.

The screening process of essential SNPs in PD

The screening processes of essential genetic variants from 72 SNPs assayed in PPMI database were shown in **Figure 1**. The essential SNPs identified by our study will exhibit the characteristics shown below: (i) The SNP is associated with PD risk according to previous genetics studies (Chang et al., 2017; Chen et al., 2016; International Parkinson Disease Genomics et al., 2011; Nalls et al., 2019; Satake et al., 2009); (ii) The SNP shows eQTL effect according to GTEx database (https://www.gtexportal.org/home/); (iii) The SNP is associated with clinical manifestations or network metrics of functional and structural networks in PD.

Identification of genetic risk variants

At first, we identified 36 SNPs conferring risk of PD from 72 SNPs examined in PPMI database according to previous literature, SNP database of NCBI (https://www.ncbi.nlm.nih.gov/snp/), and PDGene database (http://www.pdgene.org/). With the exception of *COMT* rs4680, which was shown to be associated with PD in small samples, all remaining 35 SNPs have been reported as genetic variants conferring risk of PD in previous large-scale genome-wide association studies (Chang et al., 2017; Chen et al., 2016; International Parkinson Disease Genomics et al., 2011; Nalls et al., 2019; Satake et al., 2009). For example, recent studies have confirmed that *GPNMB* rs199347 was significantly associated with PD (Chang et al., 2017; Diaz-Ortiz et al., 2022). We excluded rare mutations such as *GBA* L444P mutation (rs421016) and *SNCA* A30P mutation (rs104893878) as they were not suitable for subsequent association analysis.

Identification of risk variants associated with brain gene expressions

Based on the GTEx Project (https://www.gtexportal.org/home/), we examined whether 36 SNPs associated with PD risk were significantly correlated with gene expressions in multiple brain regions. Of 36 SNPs assessed, a total of 14 SNPs were shown to be associated with brain gene expressions. The 14 SNPs were located in 14 loci of the genome, including *OGFOD2/CCDC62* rs11060180, *GCH1* rs11158026, *ZNF646/KAT8/BCKDK* rs14235, *COMT* rs4680, *BIN3* rs2280104, *NUCKS1* rs823118, *MAPT* rs17649553, *LRRK2* rs76904798, *GALC/GPR65* rs8005172, *ZNF184* rs9468199, *FAM47E/STBD1* rs6812193, *TMEM163* rs6430538, *NCKIPSD* rs12497850, and *GPNMB* rs199347 (**Table supplement 2**). The genotype distribution of 14 SNPs in our participants didn't deviate Hardy-Weinberg equilibrium (all $p > 0.05$, X^2 test). In addition, the distribution of genotype was not significantly

different with regard to age, sex, and disease duration ($p > 0.05$). Of 14 SNPs, six of them, including *MAPT* rs17649553, *ZNF646/KAT8/BCKDK* rs14235, and *NCKIPSD* rs12497850, dramatically modified the gene expressions of multiple brain regions, including caudate, hippocampus, substantia nigra, and cortex according to GTEx project (**Figure supplement 1**). To understand the biological pathways and cellular functions associated with 14 SNPs, we used STRING database to construct the protein-protein interaction (PPI) network of differentially expressed genes and performed functional enrichment analysis to reveal the biological processes, local network cluster, cellular components, and molecular functions associated with the PPI network. As shown in **Figure supplement 2**, we found these SNPs were associated with molecular pathways involved in endocytosis, autophagy, lysosome, mitochondria metabolism, nuclear pore complex, gene transcription, and synaptic vesicles.

Associations between 14 SNPs and clinical variables

Multivariate regression analysis using 14 SNPs for genotype-phenotype associations was shown in **Table supplement 2**. We found most associations between genotypes and clinical variables had low effect sizes and did not reach the p threshold of 0.00026 (0.05/14 clinical variables x 14 SNPs), except that *GCH1* rs11158026 was significantly associated with striatal binding ratios of bilateral striatum ($\beta = -0.16$, $p = 0.0002$).

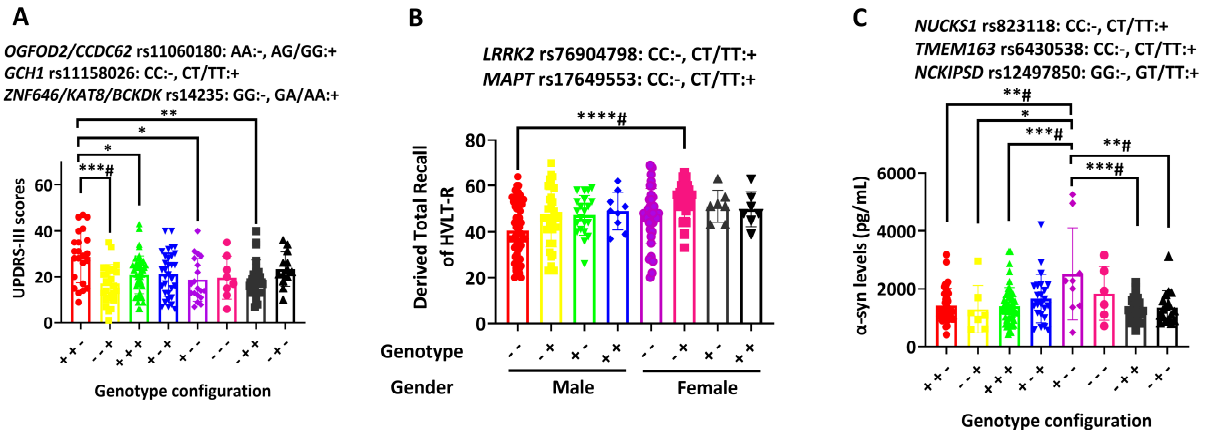

Figure 2. Multi-SNP predictive models for clinical assessments of PD. (A) Multi-SNP predictive model for UPDRS-III scores (n = 23 for ++-, n = 27 for --+, n = 48 for +++, n = 32 for +-+, n = 19 for +--, n = 8 for ---, n = 25 for -++, n = 13 for -+-). (B) Multi-SNP predictive model for Derived Total Recall T-Score of HVLT-R (Male: n = 61 for --, n = 33 for -+, n = 21 for +-, n = 9 for ++; Female: n = 35 for --, n = 25 for -+, n = 7 for +-, n = 7 for ++). (C) Multi-SNP predictive model for α-syn (α-synuclein) level in CSF (n = 39 for ++-, n = 7 for --+, n =

51 for +++, n = 23 for +-+, n = 9 for +--, n = 6 for ---, n = 26 for -++, n = 17 for -+-). Data were shown as mean ± SD. ANOVA test was used to compare the difference of clinical assessments among different genotype configurations with Tukey post-hoc test for multiple comparisons. $p < 0.05$ was considered statistically significant. * $p < 0.05$, ** $p < 0.01$, *** $p < 0.001$, **** $p < 0.0001$, # adjusted $p < 0.0036$. HVLT-R, Hopkins Verbal Learning Test – Revised; UPDRS-III, Unified Parkinson's Disease Rating Scale Part III.

Multi-SNP prediction models of PD

Though the statistical power of associations between these SNPs and clinical variables is low, we found several clinical variables, such as scores of UPDRS-III, were associated with multiple small-effect SNPs based on multivariant regression analysis (**Table supplement 2**). These findings indicate that multiple SNPs with small effect size may synergistically contribute to the variation of clinical features of PD patients. Here, we created multi-SNP models to evaluate whether the combinations of SNPs with low effect size can effectively predict the clinical presentations of PD patients. As shown in **Table supplement 2**, *OGFOD2/CCDC62* rs11060180 G allele (β = 2.71, $p < 0.01$) and *GCH1* rs11158026 T allele (β = 2.27, $p < 0.05$) were associated with higher UPDRS-III scores, while *ZNF646/KAT8/BCKDK* rs14235 A allele (β = -2.30, $p < 0.05$) was associated with lower UPDRS-III scores. Thus, PD patients can be classified into 8 groups according to the genotypes of these SNPs. As shown in **Figure 2A**, the combination of *OGFOD2/CCDC62* rs11060180 (A > G: AA, AG/GG), *GCH1* rs11158026 (C > T: CC, CT/TT), and *ZNF646/KAT8/BCKDK* rs14235 (G > A: GG, GA/AA) could predict the UPDRS-III scores of PD patients with specific genetic configuration (**Figure 2A**). Those PD patients with AG/GG+CT/TT+GG genotype had highest UPDRS-III scores (28.65 ± 11.30), while PD patients with AA+CC+GA/AA genotype had lowest UPDRS-III scores (17.07 ± 8.19, **Figure 2A**). The difference of UPDRS-III scores between these 2 groups was 11.58 ($p < 0.001$, One-way ANOVA test). Similarly, we found the combination of *LRRK2* rs76904798 T allele (β = 4.07, $p < 0.05$; C > T: CC, CT/TT) and *MAPT* rs17649553 T allele (β = 4.76, $p < 0.01$; C > T: CC, CT/TT) predicted higher Derived Total Recall T-Score of HVLT-R in a gender-dependent manner (**Figure 2B**). Female patients with CC+CT/TT genotypes had higher Derived Total Recall T-Score compared to male patients with CC+CC genotype ($p < 0.0001$, Two-way ANOVA test). Furthermore, the genotype combination of *NUCKS1* rs823118 (β = 215.40, $p < 0.05$; C > T: CC, CT/TT), *TMEM163* rs6430538 (β = -161.00, $p < 0.05$; C > T: CC, CT/TT), and *NCKIPSD* rs12497850 (β = -188.80, $p < 0.05$; G > T: GG,

GT/TT) significantly predicted α-syn level in CSF (**Figure 2C**). Patients with CT/TT+CC+GG genotype had higher α-syn level compared to patients with CC+CT/TT+GT/TT genotype who exhibited lowest α-syn level ($p < 0.001$, One-way ANOVA test). To further demonstrate our hypothesis that the clinical features of PD can be predicted by multiple SNPs, we computed PRS based on 13 SNPs of 14 functional SNPs except *COMT* rs4680, which was associated with PD risk in small case-control studies (Bialecka et al., 2012; Tang et al., 2019). We found PRS were significantly associated with rigidity scores ($\beta = -2.418$, $p < 0.01$), UPDRS-III scores ($\beta = -5.510$, $p < 0.05$), ESS scores ($\beta = -2.403$, $p < 0.05$), RBDSQ scores ($\beta = -2.268$, $p < 0.01$), and SCOPA-AUT scores ($\beta = -4.463$, $p < 0.01$). Thus, polygenic models based on multiple SNPs could also predict several clinical assessments of PD patients.

Group difference of resting-state networks

The flowchart of structural and functional network analysis was shown in **Figure supplement 3.** The independent component compositions of 5 resting-state networks were described in **Figure supplement 4**. As shown in **Figure 3A**, 10 SNPs were associated with differential network activity of resting-state networks based on the threshold of FDR corrected $p < 0.05$. If the threshold of $p < 0.0007$ (0.05/ 5 networks x 14 SNPs) after FDR correction was applied, *GPNMB* rs199347 was shown to modify the activity of SMN ($p < 0.0007$, FDR corrected, **Figure 3B**). As shown in **Figure 3B**, *GPNMB* rs199347 GG carriers exhibited higher SMN activity compared to AA carriers ($p < 0.0007$, FDR corrected; n = 26 for AA carriers and n = 11 for GG carriers). There was no significant difference in SMN activity between AA carriers and AG carriers or between AG carriers and GG carriers ($p > 0.0007$, FDR corrected; n = 26 for AA carriers, n = 37 for AG carriers, n = 11 for GG carriers). Thus, *GPNMB* rs199347 is the only SNP exerting significant impacts on resting-state networks and we focused on the effects of *GPNMB* rs199347 on neuroimaging metrics in the following analysis.

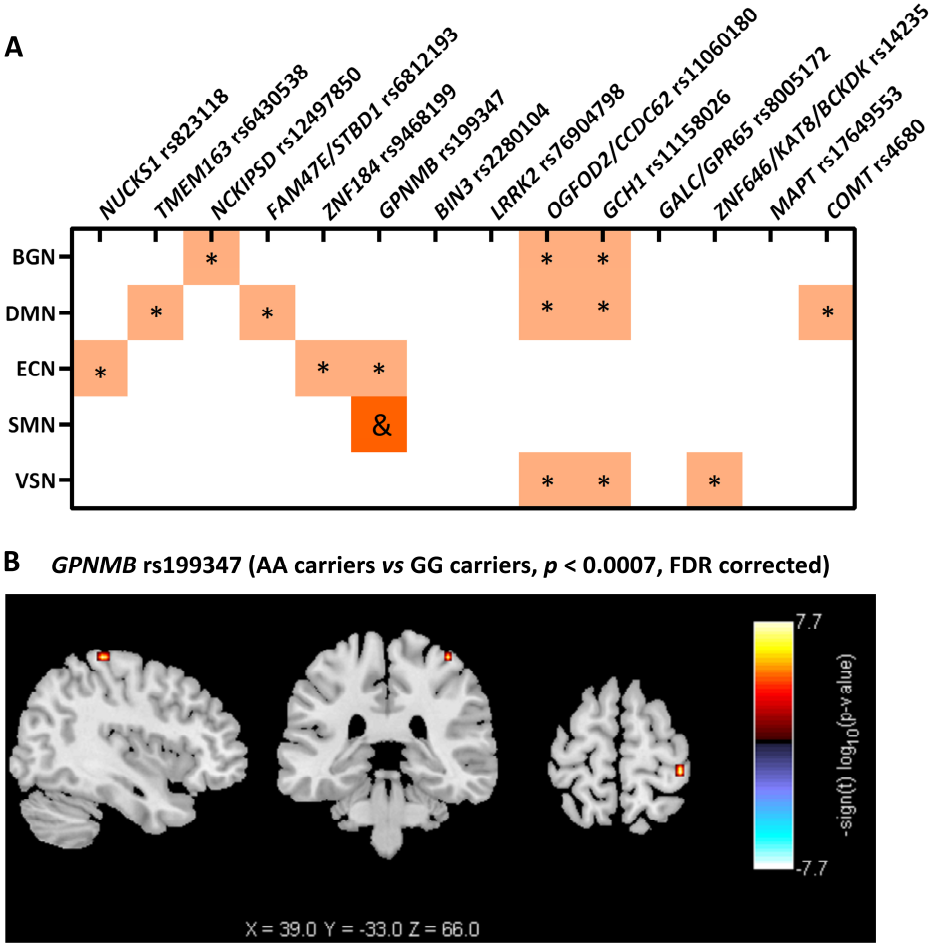

Figure 3. Group difference of resting-state networks. (A) The effects of 14 SNPs on spatial maps of five resting-state networks were evaluated using Mancovan analysis with age, sex, disease duration, and genotypes of 14 SNPs as covariates (n = 74). (B) *GPNMB* rs199347 GG carriers exhibited higher SMN activity compared to AA carriers ($p < 0.0007$, FDR corrected; n = 26 for AA carriers, n = 37 for AG carriers, and n = 11 for GG carriers). * $p < 0.05$ (FDR corrected), $^{\&}p < 0.0007$ (0.05/70, FDR corrected). BGN, basal ganglia network; DMN, default mode network; ECN, executive control network; SMN, sensorimotor network; VSN, visuospatial network.

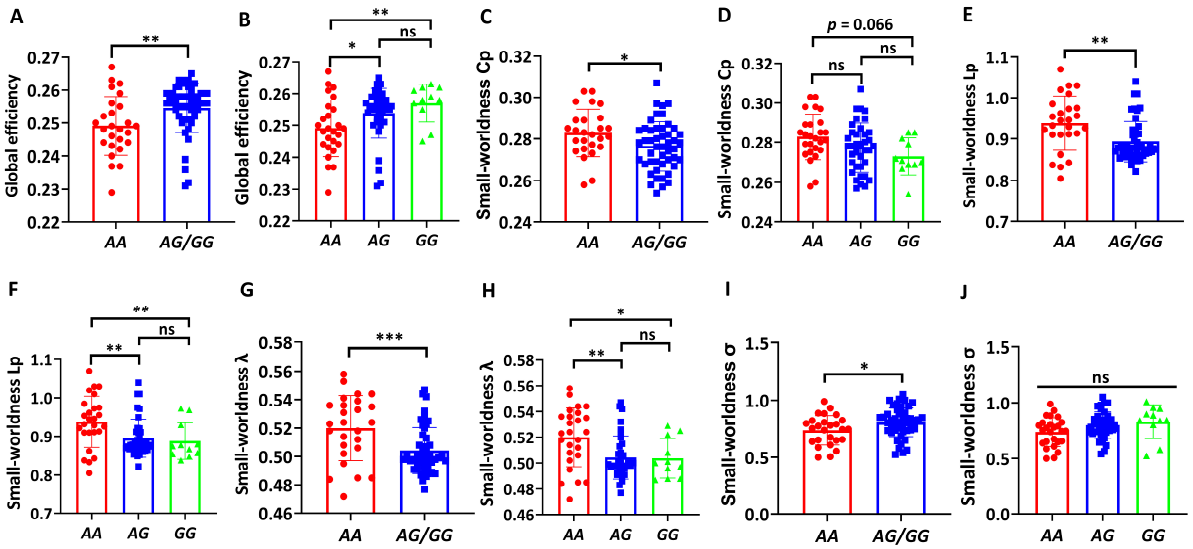

Figure 4. *GPNMB* rs199347 modifies the global network metrics of functional network. (A-J) Group difference of topological metrics of functional network, including global efficiency (A-B), small-worldness Cp (C-D), small-worldness Lp (E-F), small-worldness λ (G-H), and small-worldness σ (I-J). Data were shown as mean ± SD. The group differences of global graphical network metrics between 2 genotype groups of *GPNMB* rs199347 were analyzed using unpaired t-test (n = 26 for AA carriers, n = 48 for AG/GG carriers). The group differences of global graphical network metrics among 3 genotype groups of *GPNMB* rs199347 were analyzed using ANOVA test followed by FDR correction (n = 26 for AA carriers, n = 37 for AG carriers, and n = 11 for GG carriers). Results with $p < 0.05$ were considered statistically significant. * $p < 0.05$, ** $p < 0.01$, *** $p < 0.001$. Cp, clustering coefficient; Lp, characteristic path length.

The effects of *GPNMB* rs199347 on graphical network metrics

We assessed whether *GPNMB* rs199347 was associated with graphical network metrics of functional network. We found *GPNMB* rs199347 G-carriers (AG/GG) exhibited higher global efficiency in functional network compared to AA carriers (G-carriers: 0.255 ± 0.008 *vs* AA carriers: 0.249 ± 0.009, $p < 0.01$, unpaired t-test; n = 26 for AA carriers and n = 48 for AG/GG carriers; **Figure 4A**). Specifically, global efficiency in functional network of GG carriers was higher than that of AA carriers but not AG carriers (AA carriers: 0.249 ± 0.009 *vs* AG carriers: 0.254 ± 0.008 *vs* GG carriers: 0.257 ± 0.006, ANOVA test; n = 26 for AA carriers, n = 37 for AG carriers, and n = 11 for GG carriers; **Figure 4B**). In contrast, GG carriers or G-carriers showed reduced small-worldness Cp (GG carriers:0.273 ± 0.009 or G-carriers:0.277 ± 0.012

vs AA carriers: 0.283 ± 0.011), small-worldness Lp (GG carriers: 0.888 ± 0.047 or G-carriers: 0.894 ± 0.049 *vs* AA carriers: 0.938 ± 0.066), and small-worldness λ (GG carriers: 0.504 ± 0.015 or G-carriers: 0.504 ± 0.016 *vs* AA carriers: 0.520 ± 0.023) and increased small-worldness σ (GG carriers: 0.831 ± 0.151 or G-carriers: 0.808 ± 0.127 *vs* AA carriers: 0.738 ± 0.129) compared to AA carriers (n = 26 for AA carriers, n = 37 for AG carriers, and n = 11 for GG carriers; **Figure 4C-J**).

Then we evaluated whether *GPNMB* rs199347 carriers also shaped nodal network metrics of 90 nodes in the AAL atlas. We found *GPNMB* rs199347 GG carriers (n = 26 for AA carriers, n = 37 for AG carriers, and n = 11 for GG carriers) presented increased nodal Cp (Left caudate: AA carriers: 0.206 ± 0.118 *vs* AG carriers: 0.237 ± 0.128 *vs* GG carriers: 0.293 ±0.044, Right caudate: AA carriers: 0.217 ± 0.117 *vs* AG carriers: 0.232 ± 0.124 *vs* GG carriers: 0.277 ± 0.068; **Figure 5A**), nodal efficiency (Left caudate: AA carriers: 0.151 ± 0.077 *vs* AG carriers: 0.166 ± 0.081 *vs* GG carriers: 0.209 ± 0.040, Right caudate: AA carriers: 0.146 ± 0.075 *vs* AG carriers: 0.162 ± 0.079 *vs* GG carriers: 0.205 ± 0.032; **Figure 5B**), and nodal local efficiency (Left caudate: AA carriers: 0.238 ± 0.130 *vs* AG carriers: 0.266 ± 0.142 *vs* GG carriers: 0.347 ± 0.041, Right caudate: AA carriers: 0.244 ± 0.127 *vs* AG carriers: 0.260 ± 0.136 *vs* GG carriers: 0.327 ± 0.057; **Figure 5C**) in bilateral caudate of functional network compared to AA carriers and AG carriers (n = 26 for AA carriers, n = 37 for AG carriers, and n = 11 for GG carriers). Consistently, *GPNMB* rs199347 GG carriers had reduced nodal shortest path length in bilateral caudate compared to AA carriers and AG carriers (Left caudate: AA carriers: 11.189 ± 11.119 *vs* AG carriers: 10.081 ± 12.353 *vs* GG carriers: 2.839 ± 2.081, Right caudate: AA carriers: 11.300 ± 11.079 *vs* AG carriers: 10.692 ± 12.510 *vs* GG carriers: 2.839 ± 2.017; **Figure 5D**).

GPNMB rs199347 was not associated with significant changes of graphical metrics in white matter network and gray matter covariance network (data not shown).

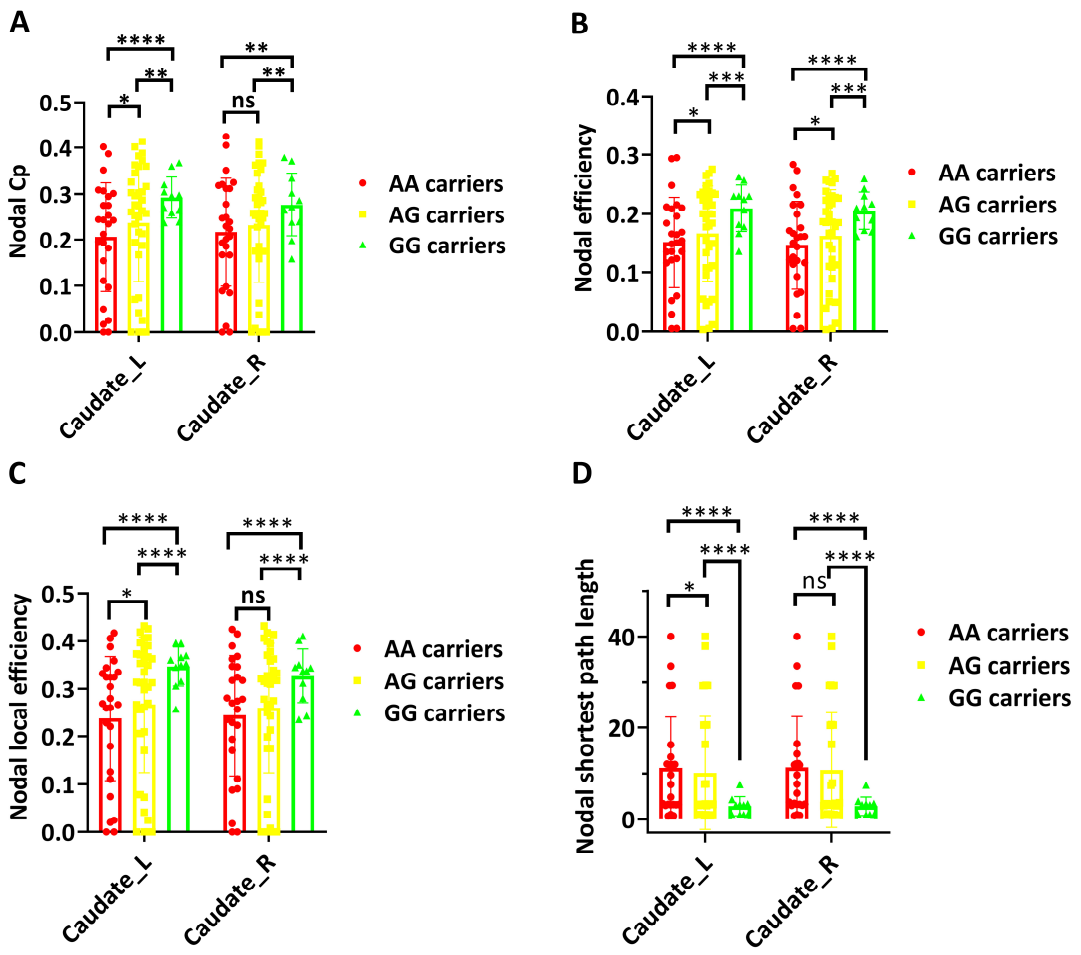

Figure 5. *GPNMB* rs199347 specifically shapes the nodal network metrics of bilateral caudate. (A-D) Increased nodal clustering coefficient (A), nodal efficiency (B), and nodal local efficiency (C) in AG/GG carriers compared to AA carriers. Reduced nodal shortest path length (D) in AG/GG carriers compared to AA carriers (n = 26 for AA carriers, n = 37 for AG carriers, and n = 11 for GG carriers). Data were shown as mean ± SD. The group differences of nodal graphical network metrics among 3 genotype groups of *GPNMB* rs199347 were analyzed using ANOVA test. Results with $p < 0.05$ after FDR correction were considered statistically significant. * $p < 0.05$, ** $p < 0.01$, *** $p < 0.001$, **** $p < 0.0001$. Cp, clustering coefficient.

To adjust the confounding factors, we utilized multivariate regression models to assess the effects of *GPNMB* rs199347 on both global and nodal network metrics of functional network. The covariates included age, sex, disease duration, and genotypes of other 13 SNPs (n =74). For global network metrics, we found *GPNMB* rs199347 was significantly associated with global efficiency ($\beta = 0.0045$, $p < 0.01$), small-worldness Lp ($\beta = -0.0310$, $p < 0.01$), small-worldness γ ($\beta = 0.0862$, $p < 0.01$), small-worldness λ ($\beta = -0.0094$, $p < 0.01$), and small-worldness σ ($\beta = 0.0763$, $p < 0.01$) of functional network. For nodal network metrics, *GPNMB*

rs199347 was significantly associated with nodal Cp (Left caudate: $\beta = 0.0478$, $p < 0.05$; Right caudate: $\beta = 0.0421$, $p < 0.05$), nodal efficiency (Left caudate: $\beta = 0.0235$, $p = 0.08$; Right caudate: $\beta = 0.0232$, $p = 0.08$), nodal local efficiency (Left caudate: $\beta = 0.0527$, $p < 0.05$; Right caudate: $\beta = 0.0463$, $p < 0.05$), and nodal shortest path length (Left caudate: $\beta = -4.2480$, $p = 0.06$; Right caudate: $\beta = -4.1940$, $p = 0.06$) of bilateral caudate. Thus, the effects of *GPNMB* rs199347 on both global and nodal network metrics were independent of age, sex, disease duration, and genotypes of other 13 SNPs.

Comparison of global connectivity strength

To further evaluate the effects of *GPNMB* rs199347 on brain networks, we used NBS method to assess how *GPNMB* rs199347 modify the global connectivity strength of functional networks and structural networks. However, *GPNMB* rs199347 was not found to be associated with the global connectivity strength of brain networks (5000 permutations, FDR corrected $p > 0.05$).

Comparisons of gray matter structure and white matter integrity

We also evaluated whether *GPNMB* rs199347 modified the gray matter and white matter structure of PD patients. We found *GPNMB* rs199347 had no significant effects on the gray matter volume and cortical thickness of PD patients (FDR corrected $p > 0.05$, data not shown). Additionally, *GPNMB* rs199347 was also not shown to modify the integrity of white matter tracts (FDR corrected $p > 0.05$, data not shown).

Discussion

In current study, we found 14 PD-associated SNPs, including *GPNMB* rs199347, were eQTLs and associated with multiple biological pathways involved in endocytosis-autophagy-lysosome, mitochondria, gene transcription, and nuclear pore complex. Interestingly, we also found specific combinations of some SNPs in this study predicted clinical assessments of PD patients. In addition, we revealed *GPNMB* rs199347 G allele enhanced the activity of SMN. Furthermore, *GPNMB* rs199347 G allele also specifically increased the efficiency of global and local information transfer in functional network using graphical analysis. Our findings highlight the protective effects of *GPNMB* rs199347 on the functional network of PD patients, which may provide partial explanations for *GPNMB* rs199347 as a protecting genetic locus in PD (OR =0.90) (Chang et al., 2017).

To date, a large number of SNPs have been identified to be associated with the risk of PD, nevertheless, the underlying neural mechanisms of previously reported SNPs were largely unknown (Chang et al., 2017; Nalls et al., 2019). Some preliminary studies have identified PD-associated SNPs were associated with common pathological pathways in PD, such as endocytosis, autophagy, lysosome, mitochondria metabolism, immunological surveillance, DNA replication, synaptic vesicle recycling, and microtubule polymerization (Chang et al., 2017; Cui, Xu, Zhang, & Wang, 2021; Farrow et al., 2022), which were consistent with our functional enrichment results (**Figure supplement 2**) based on PPI network derived from differentially expressed genes. Interestingly, we found nuclear pore complex was a new biological pathway associated with PD-associated SNPs. In fact, altered nucleocytoplasmic transport has been thought as an emerging pathomechanism of multiple neurodegenerative diseases, including amyotrophic lateral sclerosis, Alzheimer disease (AD), frontotemporal dementia and Huntington disease (Coyne & Rothstein, 2022). Specific nucleoporin abnormalities occur in sporadic and familial forms of neurodegenerative disease, and the dysfunction of nuclear pore complex is thought to contribute to disrupted nucleocytoplasmic transport (Coyne et al., 2021; Coyne et al., 2020; K. Zhang et al., 2018). Whether nuclear pore complex was altered in PD and associated with PD pathogenesis remained unclear and deserved to be further explored. For *GPNMB* rs199347, according to GTEx database (https://www.gtexportal.org/home/), G allele was significantly associated with reduced expression of *GPNMB* in multiple brain regions, including cortex ($p = 1.8 \times 10^{-20}$), caudate ($p = 3.0 \times 10^{-19}$), putamen ($p = 5.5 \times 10^{-24}$), and substantia nigra ($p = 2.1 \times 10^{-5}$). In addition, *GPNMB* rs199347 G allele was also significantly associated with reduction of *NUPL2* expression in cortex ($p = 5.0 \times 10^{-17}$), caudate ($p = 6.6 \times 10^{-10}$), putamen ($p = 5.6 \times 10^{-8}$), and substantia nigra ($p = 1.3 \times 10^{-11}$). Consistently, Diaz-Ortiz et al. (2022) demonstrated that individuals carrying two different alleles for *GPNMB* rs199347 haplotype exhibited allele-specific expression for *GPNMB* (Diaz-Ortiz et al., 2022). They also confirmed that moderate to high levels of GPNMB protein are expressed in the human brain of multiple postmortem cases by immunoblotting and immunohistochemistry (Diaz-Ortiz et al., 2022). Because higher expression of GPNMB conferred pathogenicity in PD (Diaz-Ortiz et al., 2022), G allele was protective for the reductions of *GPNMB* levels in G-carriers of PD. Considering that GPNMB expression was found in multiple cell types of the brain (Diaz-Ortiz et al., 2022), future studies were required to dissect its role in the modulation of brain function.

Accumulating evidence has demonstrated that most of the traits or phenotypes in humans were affected by multiple genetic variants (Backman et al., 2021; Vuckovic et al., 2020; White et al., 2021) and our study also supports this notion. Although single genetic variant in our study is not significantly associated with clinical manifestations of PD patients after multiple comparisons, multi-SNP models exhibited high predictive power for some clinical assessments. We revealed that the specific genotype configuration combining *OGFOD2/CCDC62* rs11060180, *GCH1* rs11158026, and *ZNF646/KAT8/BCKDK* rs14235 outstandingly predicted the UPDRS-III scores of PD patients, indicating that motor symptoms of PD patients were shaped by multiple genetic variants. Additionally, we revealed *MAPT* rs17649553 and *LRRK2* rs76904798 were found to synergistically protect PD patients from verbal memory impairment with a gender-dependent manner. We also found that α-syn level in CSF can be affected by three SNPs, including *NCKIPSD* rs12497850, *NUCKS1* rs823118, and *TMEM163* rs6430538. The significant correlations between PRS and clinical assessments also suggest that the clinical features of PD patients were shaped by multiple genetic variants. Importantly, the effects of individual SNP on clinical assessments were independent of age, sex, disease duration, and genotypes of other 13 SNPs. Taken together, our novel findings support a polygenic basis underlying the clinical heterogeneity of PD patients (Nalls et al., 2019). Because 4 SNPs (*NCKIPSD* rs12497850, *NUCKS1* rs823118, *MAPT* rs17649553, and *ZNF646/KAT8/BCKDK* rs14235) significantly predicting clinical assessments also exhibited dramatical eQTL effects ($p < 0.0001$, **Figure supplement 1**), these SNPs deserved to be further investigated in future studies. As shown in **Table supplement 2**, *GPNMB* rs199347 was not significantly correlated with motor symptoms and striatum SBRs, therefore, *GPNMB* rs199347 may have no effects on motor functions of PD patients.

Using ICA, we revealed that *GPNMB* rs199347 GG genotype exhibited enhanced SMN activity which was found to be disrupted in PD (Caspers et al., 2021), indicating that *GPNMB* rs199347 was a protective genetic variant to preserve the integrity of SMN in PD. Because we included age, sex, disease duration, and genotypes of other 13 SNPs as covariates during the mancovan analysis, the protective role of *GPNMB* rs199347 G allele in SMN integrity was independent of individual demographical factors and also other genetic variants investigated by our study. Currently, studies assessing the effects of genetic variation on resting-state networks of humans were scarce (Zhao et al., 2022), thus our study provided preliminary results that resting-state networks could be modified by PD-associated genetic variants.

The disruption of network topology was an essential hallmark of PD (Fang et al., 2017; Guo et al., 2020; Ji et al., 2019; Luo et al., 2015; Wei et al., 2014; D. Zhang, Wang, Liu, Chen, & Liu, 2015). However, no studies have ever explored whether PD-associated SNPs modified the network topology of the patients. In this study, we elucidated that both global network metrics and nodal network metrics of functional network were differentially affected by *GPNMB* rs199347. *GPNMB* rs199347 GG carriers had increased global efficiency of functional network compared to AA carriers, indicating G allele was associated with higher efficiency of information transfer within functional network of PD, which is consistent with lower small-worldness Lp and small-worldness λ in GG carriers. The increased small-worldness σ in G-carriers also suggested that *GPNMB* rs199347 G allele is protective in PD by improving the global efficiency of information transfer within functional networks (Latora & Marchiori, 2001). In addition, *GPNMB* rs199347 G allele specifically increased the nodal efficiency and nodal local efficiency and reduced nodal shortest path length of bilateral caudate, further indicating that *GPNMB* rs199347 G allele was associated with higher efficiency of local information transfer of bilateral caudate compared to A allele. Thus, our results supported that *GPNMB* rs199347 is protective in PD by improving global and local information processing of functional networks. Because the structural networks were not affected by *GPNMB* rs199347, we concluded that *GPNMB* rs199347 specifically shaped resting-state networks in PD without effects on structural networks. According to the results in **Table supplement 2**, *GPNMB* rs199347 was not significantly associated with clinical features of PD patients, thus *GPNMB* rs199347 G allele carriers are more prone to the changes of functional network but not clinical phenotypes of PD patients.

GPNMB is a glycoprotein associated with tissue damage and inflammation and plays a key role in the regulation of inflammatory responses of astrocyte, microglia, and macrophage (Budge, Neal, Richardson, & Safadi, 2020; Neal, Boyle, Budge, Safadi, & Richardson, 2018; Robinet et al., 2021). In PD, *GPNMB* rs199347 has been demonstrated to be a key genetic locus of PD and associated with α-syn pathology (Chang et al., 2017; Diaz-Ortiz et al., 2022) and the expression of GPNMB is selectively enhanced in the substantia nigra of PD patients and increases after lysosomal stress (Moloney, Moskites, Ferrari, Isacson, & Hallett, 2018). Diaz-Ortiz et al. (2022) reported that *GPNMB* significantly modified synaptic biology, including synapse assembly, synapse organization, and synapse signaling (Diaz-Ortiz et al., 2022). This may provide explaination for the effects of *GPNMB* rs199347 on functional network, which is associated with synaptic structure and function (Bennett, Farnell, & Gibson,

2008; Jessen et al., 2015; Kahali, Raichle, & Yablonskiy, 2021; Xu et al., 2021). It should be noted that they also found GPNMB was necessary for internalization of fibrillar α-syn and contributes to development of α-syn pathology (Diaz-Ortiz et al., 2022). Therefore, they concluded that higher expression of *GPNMB* contributed to neuronal pathogenicity through interactions with α-syn. Because GG carriers had reduced level of GPNMB expression compared to AA carriers (Diaz-Ortiz et al., 2022), their results suggested that G allele is protective in PD, which is consistent with our findings. However, in another study, GPNMB was not found to be associated with synucleinopathy because GPNMB level was not altered in mice models of synucleinopathy (Moloney et al., 2018). This result was supported by a recent study showing that *GPNMB* deletion had no effect on cellular, histological, and behavioral phenotypes of two models of α-syn pathology (Brendza et al., 2021). Because of the controversial findings related to *GPNMB* and synucleinopathy, more endeavors were required to decode the role of *GPNMB* in the initiation and progression of PD.

In conclusion, our findings suggest that PD risk-associated SNPs, including *GPNMB* rs199347, were significantly correlated with brain gene expressions. Further studies will be recommended to dissect the molecular mechanisms associated with these SNPs. Additionally, our neuroimaging findings strongly support that G allele of *GPNMB* rs199347 is a protective allele for PD, specifically enhancing the activity of SMN and the information transfer efficiency of functional network. Future studies are needed to examine the role of this genetic variant in PD pathogenesis and progression.

Materials and methods

Participants

The data used in the preparation of this Article were obtained from PPMI database, which is a robust open-access online resource platform, providing clinical, imaging, 'omics, genetic, sensor, and biomarker data set to deepen the understanding of PD and speed scientific breakthroughs and new treatments. The data collection protocols for PPMI have been published and available online (http://www.ppmi-info.org/) (Marek et al., 2018; Parkinson Progression Marker, 2011). The PPMI study was approved by institutional review boards at each participating site, and all participants completed written informed consent before they were enrolled. The inclusion criteria for participants in PPMI cohort has been published previously (Marek et al., 2018). For the purposes of our study, only participants who underwent 3D T1

imaging or resting-state fMRI or diffusion tensor imaging (DTI) were selected for data analysis. Because only a small percentage of control participants received MRI examinations, they were not included in the neuroimaging analysis. A total of 198 PD patients were identified to have 3D T1 images. Of these PD patients, 146 and 83 underwent DTI and resting-state fMRI, respectively. The investigators of this study (Jun Liu and Zhichun Chen) visually inspected the MRI images of selected patients to ensure that neither T1-weighted nor T2-weighted images had evidence of structural abnormalities. In addition, almost all the patients performed iodine-123-labelled ioflupane SPECT to measure DAT activity. Volume of interest were placed on the left and right caudate, left and right putamen, and the occipital cortex (reference tissue) to extract the count densities for each of the four striatal regions (Marek et al., 2018). Striatal binding ratios (SBR) of caudate and putamen were calculated as (target region/reference region)-1 (Marek et al., 2018). We downloaded all the SBR data from the PPMI database. Most of the participants also tested for indices in CSF, including levels of β-amyloid (Aβ), α-syn (α-synuclein), p-tau, and tau, which were also downloaded from PPMI database. The basal demographical data, motor symptoms, non-motor symptoms, SBR, and CSF indices were collected for 198 PD patients and 189 control participants (**Table supplement 1**). The control participants were required to be 30 years of age or older with no active, clinically manifested neurological disease or first-degree relatives with PD or genetic mutations of PD. Both PD and control participants were not from the genetic PPMI cohort and prodromal cohort. To ensure consistency in the timing of data collection, we kept the maximum time gap for all types of data collection within 3 months. The genotypes of 72 genetic variants detected by whole-genome sequencing in PPMI were downloaded to analyze the associations between genotypes and phenotypes in PD (http://www.ppmi-info.org/). Unpaired *t* test or X^2 test was used for the comparison of clinical variables between control and PD patients. The screening processes of essential genetic variants from 72 SNPs assayed in PPMI database were shown in **Figure 1**.

Image acquisition

All the fMRI images were acquired on 3T Siemens MRI scanners at different participating site. Most of 3D T1 MPRAGE sequence was scanned with following parameters: TR = 2300 ms, TE = 2.98 ms, Inversion time = 900 ms, Voxel size = 1 mm^3, Matrix = 240 x 256 mm, Flip Angle = 9°, Slice thickness =1.2 mm. The resting-state fMRI was acquired for 8 minutes and 24 seconds with parameters of TR = 2400 ms, TE = 25 ms, Voxel size = 3.3 mm^3, Field of View = 222 mm, Flip Angle = 80°, Slice thickness = 3.3 mm. The DTI images were performed

along 64 directions using a b-vale of 1000 s/mm^2, and a single b = 0 image. Single shot echo-planar imaging (EPI) sequence was used with following parameters: TR= 8,400-8,800 ms, TE = 88 ms, Voxel size = 2 mm^3, Flip Angle = 90°, Slice thickness = 2 mm. During the resting-state imaging, participants were required to stay quietly with clear mind and not to sleep.

Image preprocessing

Before all the images were preprocessed, the DICOM format images were transformed into NIFTI format images. For the preprocessing of resting-state fMRI images, the first 10 volumes were removed to achieve magnetization equilibrium. The remaining images were then slice-timing corrected and realigned. The rest of datasets were spatially normalized to Montreal Neurological Institute (MNI) space using EPI template in SPM12 (https://www.fil.ion.ucl.ac.uk/spm/software/spm12/). A 4-mm Gaussian smoothing kernel was applied to improve anatomical variance and signal to noise ratio. All voxel time series were then bandpass filtered (0.01~0.1 HZ) to emphasize the low-frequency correlations and eliminate the low-frequency drift and high-frequency noises. To adjust the head motions, six head motion parameters, signals of white matter and CSF, were regressed out from each dataset. Among 83 PD subjects with resting-state fMRI, we excluded 9 subjects with head motions frame-wise displacement > 0.5 mm and head rotation > 2°. The remaining 74 PD participants underwent functional network analysis.

For DTI analysis, we included all 146 PD subjects. Their DTI images were preprocessed using the FMRIB Software Library toolbox (FSL, https://fsl.fmrib.ox.ac.uk/fsl/fslwiki). The images preprocessing included the following major steps: (i) Removing the nonbrain tissue and extracting the brain using the Brain Extraction Tool; (ii) Correcting the eddy-current distortion and head motions using eddy_correct command; (iii) Computing the diffusion tensor metrics using dtifit command. (iv) Normalizing the images into MNI space.

The gray matter images of 198 PD subjects were preprocessed using voxel-based morphometry (VBM) methodology (Ashburner & Friston, 2000) implemented on CAT12 toolbox (Dahnke, Yotter, & Gaser, 2013) running within SPM12. Briefly, the T1 images were firstly normalized with Diffeomorphic Anatomic Registration Trough Exponentiated Lie algebra algorithm template and then segmented into gray matter, white matter, and CSF. The segmented gray matter images were further smoothed before the construction of gray matter covariance network. For surface-based morphometry (SBM), a fully automated method was

used to measure cortical thickness and reconstruct the central surface using CAT12 toolbox. Partial volume information, sulcal blurring and asymmetries were handled by projection-based thickness. The processed surface data were smoothed using 15 mm kernel (12~18mm kernels are widely used for SBM) before statistical analysis.

Network construction

We used atlas of Automated Anatomical Labeling (AAL) to define 90 cortical and subcortical nodes. The functional connectivity was calculated using the Pearson's correlation of mean time courses of the 90 nodes. To improve the normality, the Fisher's r-to-z transformation was performed. This created a 90 x 90 functional connectivity matrix for each subject.

Deterministic tractography was performed for individual preprocessed DTI images based on AAL atlas using the Fiber Assignment by Continuous Tracking (FACT) algorithm embedded in a free open Matlab toolbox PANDA (http://www.nitrc.org/projects/panda/). To construct white matter fibers, streamlines were created in each voxel along the principle diffusive direction. When the streamline reached a voxel with fractional anisotropy (FA) < 0.2 or tract angle > 45°, the streamline tracking was terminated. We used the fiber number (FN) to define structural connectivity. We didn't set the threshold for FN within network here, because the threshold didn't significantly affect the network properties. Finally, a 90 x 90 white matter FN matrix was constructed for each participant.

The methodology to construct the gray matter covariance network has been described previously (Batalle et al., 2013; Tijms, Series, Willshaw, & Lawrie, 2012). In brief, the AAL atlas was used to define the 90 subcortical and cortical nodes with 3 x 3 x 3 voxels. The network edges were computed as the correlation coefficients of gray matter volume between each pair of 90 nodes. The correlation coefficients were then Fisher's r-to-z transformed. Finally, a 90 x 90 gray matter covariance matrix was created for individual participant.

Network graphical analysis

The graph theory was used to analyze the topological properties of above three types of networks. We calculated both global and nodal metrics of networks using GRETNA toolbox (https://www.nitrc.org/projects/gretna/). The global network metrics included global efficiency, local efficiency, and small-worldness properties: clustering coefficient (Cp), characteristic path length (Lp), normalized clustering coefficient (γ), normalized characteristic

path length (λ), and small worldness (σ). The nodal metrics estimated in this study included nodal efficiency, nodal local efficiency, nodal Cp, and nodal shortest path length. We calculated the area under curve (AUC) for each network metric. The definitions and computations of above topological parameters were described below and could also be found in previous studies (Rubinov & Sporns, 2010; Wang et al., 2011). We defined *N* as the set of all nodes in a network, *n* as the number of nodes, *L* as the set of all edges (links) in the network, and *l* as the number of edges. (*i*,*j*) is a link between nodes *i* and *j*, (*i*,*j* ∈ *N*). a_{ij} is the connection status between node *i* and node *j*. a_{ij} =1 when the link between node *i* and node *j* exists, a_{ij} = 0 otherwise (a_{ij} = 0 for all *i*). The number of links is computed as $l = \sum_{i,j \in N} a_{ij}$.

The degree (k_i) is defined as the number of links connected to a node *i*, then the degree of this node *i* is computed as below:

$$k_i = \sum_{j \in N} a_{ij}$$

The shortest path length between node *i* and node *j* is computed as below:

$$d_{ij} = \sum_{a_{uv} \in gi \leftrightarrow j} a_{uv}$$

$gi \leftrightarrow j$ is the shortest path between node *i* and node *j*.

The nodal shortest path length is the average shortest path length between node *i* and all other nodes. It is computed as below:

$$L_i = \frac{\sum_{j \in N, j \neq i} dij}{n-1}$$

The node local efficiency measures the efficiency of local information transfer in node *i*. The node local efficiency is computed as below:

$$E(i) = \frac{1}{n_{G_i}(n_{G_i} - 1)} \sum_{j \neq k \in G_i} \frac{1}{d_{j,k}}$$

G_i is the Graph composed of neighbor nodes of node *i*. $d_{j,k}$ represents shortest path length between node *j* and node *k*.

The node efficiency measures the efficiency of information transfer for node *i* in the network. Node efficiency is computed as below:

$$E_i = \frac{1}{n-1} \sum_{i,j \in N, i \neq j} \frac{1}{d_{ij}}$$

$d_{j,k}$ represents shortest path length between node *j* and node *k.*

The global efficiency is defined as the average E_i of all nodes in a network. It is computed as below:

$$E_{global} = \frac{1}{n(n-1)} \sum_{i,j \in N, i \neq j} \frac{1}{d_{ij}}$$

The local efficiency is defined as the average $E(i)$ of all nodes in a network. It is computed as below:

$$E_{loc} =< E(i) >= \frac{1}{n} \sum_{i \in N} E(i)$$

The node Cp measures how closely nodes in a network tend to group together. It is computed as below:

$$C_i = \frac{2e_i}{k_i(k_i - 1)}$$

The network Cp is the average node Cp of a network and is computed as below:

$$C =< C_i >= \frac{1}{n} \sum_{i \in N} \frac{2e_i}{k_i(k_i - 1)}$$

Characteristic path length (Lp) of the network is defined as the average shortest path length of all nodes in a network. It is computed as below:

$$L = \frac{1}{n} \sum_{i \in N} L_i = \frac{1}{n} \sum_{i \in N} \frac{\sum_{j \in N, j \neq i} dij}{n-1}$$

where *Li* is the average shortest path length between node *i* and all other nodes.

The small-worldness γ is computed as below:

$$\gamma = \frac{C_{brain}}{C_{random}}$$

where C_{brain} and C_{random} represents the Cp of brain network and random network, respectively.

The small-worldness λ is computed as below:

$$\lambda = \frac{L_{brain}}{L_{random}}$$

where L_{brain} and L_{random} represents the L (Characteristic path length) of brain network and random network, respectively.

The small-worldness σ is computed as below:

$$\sigma = \frac{\gamma}{\lambda}$$

Identification of resting-state networks

The Group ICA of fMRI Toolbox (GIFT v4.0a; http://icatb.sourceforge.net) was used to extract the five functional networks. The independent component analysis (ICA) included three major steps: (i) Data reduction using principal component analysis; (ii) Application of the ICA algorithm; (iii) Back reconstruction for subject components. The number of independent components (ICs) was determined using the minimum description length criteria (Y. O. Li, Adali, & Calhoun, 2007). After ICA, the functional images of each participant were reduced to 100 ICs, thirty-three of which were finally selected to create the 5 resting-state networks, including default mode network (DMN: IC28, IC38, IC41, IC45, IC46, IC49, IC77, IC95, and IC98), basal ganglia network (BGN: IC9, IC14, IC30, IC33, IC82), executive control network (ECN: IC34, IC51, IC55, IC58, IC62), sensorimotor network (SMN: IC16, IC18, IC42, IC48, IC53, IC67, IC89, and IC91), and visuospatial network (VSN: IC19, IC64, IC80, IC85, IC87, and IC100). The compositions of ICs for five resting-state networks were shown in **Figure supplement 4**.

The acquisition of eQTL data

All the eQTL data of analyzed SNPs were obtained from the Genotype-Tissue Expression (GTEx, https://www.gtexportal.org/home/) Project. The normalized effect size (NES) was computed as the effect of the alternate allele relative to the reference allele (https://www.gtexportal.org/home/faq). Uncorrected $p < 0.05$ was reported to identify the potential eQTL effect. A smaller $p < 0.0001$ was reported as higher eQTL effect.

Association analysis between phenotype assessments and genotypes

The associations between genotypes of SNPs and clinical features of PD patients were analyzed using multivariate regression models. During the multivariate regression analysis, the dependent variables (n=14) included the scores of Unified Parkinson's Disease Rating Scale part III (UPDRS-III), Epworth Sleepiness Scale (ESS), Geriatric Depression Scale, REM Sleep Behavior Disorder Screening Questionnaire (RBDSQ), Scale for Outcomes in Parkinson's Disease-Autonomic (SCOPA-AUT), Letter Number Sequencing, Montreal Cognitive Assessment (MoCA), Hopkins Verbal Learning Test-Revised (HVLT-R: Total Recall and Immediate Recall), Semantic Fluency Test, and SBRs (putamen, caudate, and striatum), as well as α-syn level in CSF. The independent variables were the genotypes of 14 SNPs**.** During the multivariate regression analysis, age, sex, disease duration, and genotypes of remaining 13 SNPs were included as covariates and β (coefficients) and p values were reported for each SNP. Because of the lack of total levodopa equivalent daily dose (LEDD) data in most PD patients, LEDD was not included as a covariate during the association analysis. The multivariate regression models were shown below (SNP_1, SNP_2, …, SNP_i represent the genotypes of SNPs):

$$Dependent\ variabels = \beta_0 + \beta_1 * Age + \beta_2 * Sex + \beta_3 * Disease\ duration + \beta_4 * SNP_1 + \beta_5 * SNP_2 + \cdots + \beta_{i+3} * SNP_i \qquad (i = 1, 2, \ldots, 14)$$

Results with $p < 0.05$ and $p < 0.00026$ (0.05/14*14; 14 clinical variables x 14 SNPs) after correction for multiple comparisons were reported.

Multi-SNP prediction models

Multivariate regression analysis was utilized to establish multi-SNP models to predict clinical assessments of PD. ANOVA test followed by Tukey post-hoc test was used to compare the difference of clinical assessments among different multi-SNP configurations. $p < 0.05$ was considered statistically significant. The derivation of polygenic risk score (PRS) based on multiple SNPs was another method to create multi-SNP prediction models according to

previous studies (Khera et al., 2018; R. Li, Chen, Ritchie, & Moore, 2020). We computed the PRS using the odds ratio of every SNP in large-scale genome-wide association studies. Because *COMT* rs4680 was found to be associated with PD risk in small case-control studies (Bialecka et al., 2012; Tang et al., 2019), it was not included for the calculation of PRS. Totally 13 SNPs were utilized to derive the PRS for individual participants. The PRS was calculated using the formulation shown below:

$$PRS = \sum_{i=1}^{n} \ln(OR_i) * N_i \quad (OR_i \text{ is the odds ratio of } SNP_i, N_i \text{ is the number of risk allele in } SNP_i)$$

The associations between clinical assessments and PRS were examined by multivariate regression models with age, sex, and disease duration as covariates.

Comparisons of resting-state networks

The comparisons of network spatial maps were performed using Mancovan analysis with age, sex, disease duration, and genotypes of 14 SNPs as covariates. The results with FDR corrected $p < 0.05$ and $p < 0.0007$ (0.05/70, 5 networks x 14 SNPs) were considered statistically significant.

Group difference of graphical network metrics

The group differences of global graphical network metrics between 2 genotype groups of *GPNMB* rs199347 were analyzed using unpaired t-test. Results with $p < 0.05$ were considered statistically significant. The group differences of global or nodal graphical network metrics among 3 genotype groups of *GPNMB* rs199347 were analyzed using ANOVA test followed by FDR correction. The nodal network metrics of 90 nodes in AAL atlas were compared among 3 genotype groups of *GPNMB* rs199347. Results with $p < 0.05$ after FDR correction were considered statistically significant.

Associations between *GPNMB* rs199347 and graphical network metrics

The multivariate regression models were used for the association analysis between genotypes of *GPNMB* rs199347 and graphical network metrics. The analyzed network metrics include: global efficiency, local efficiency, small-worldness properties (Cp, Lp, γ, λ, σ), and nodal network metrics. Age, sex, and disease duration were included as covariates during multivariate regression analysis. Results with $p < 0.05$ were considered statistically significant.

Comparisons of network strength using Network-based statistic

To compare global network strength, we used network-based statistic (NBS, https://www.nitrc.org/projects/nbs/) method with 5000 permutations(Zalesky, Fornito, & Bullmore, 2010). The age, sex, and disease duration were used as covariates during the analysis. Results with $p < 0.05$ after FDR correction were considered statistically significant.

Comparisons of gray matter volume or cortical thickness

The whole brain comparison of gray matter volume or cortical thickness among different genotype groups (AA, AG, and GG) of *GPNMB* rs199347 was performed using ANOVA models in CAT12 toolbox and SPM12. The age, sex, and disease duration were included as covariates. $p < 0.05$ after FDR correction was considered statistically different.

Comparisons of integrity of white matter tracts

The comparison of integrity (FA) of white matter tracts among different genotype groups (AA, AG, and GG) of *GPNMB* rs199347 was performed using ANOVA models. The age, sex, and disease duration were included as covariates. $p < 0.05$ after FDR correction was considered statistically different.

Acknowledgements

We thank the share of PPMI data by all the PPMI study investigators. For up-to-date information on PPMI study, visit www.ppmiinfo.org. PPMI – a public-private partnership – is funded by the Michael J. Fox Foundation for Parkinson's Research and funding partners, which can be found at www.ppmiinfo.org/fundingpartners.

Additional information

Competing interests

The other authors declare that no competing interests exist.

Funding

Funder	Grant reference number	Author
National Key Research and Development Program	2016YFC1306505	Jun Liu
National Natural Science Foundation of China	81471287	Jun Liu
National Natural Science Foundation of China	81071024	Jun Liu
National Natural Science Foundation of China	81171202	Jun Liu

The funders had no role in study design, data collection and interpretation, or the decision to submit the work for publication.

Author contributions

Zhichun Chen, Conceptualization, Formal analysis, Visualization, Methodology, Writing - original draft, Writing - review and editing; Bin Wu, Validation, Investigation, Methodology; Guanglu Li, Data curation, Formal analysis, Visualization; Liche Zhou, Data curation, Formal analysis, Investigation; Lina Zhang, Formal analysis, Investigation, Methodology; Jun Liu, Conceptualization, Supervision, Funding acquisition, Writing - original draft, Project administration, Writing- review and editing.

Ethics

The PPMI study was conducted in accordance with the Declaration of Helsinki and the Good Clinical Practice (GCP) guidelines after approval of the local ethics committees of the participating sites.

Supplementary files

The supplementary files included 2 supplementary tables and 4 supplementary figures.

Data availability

All the raw data used in the preparation of this Article were downloaded from PPMI database (www.ppmi-info.org/data). All data produced in the present study are available upon reasonable request to the authors.

References

Ashburner, J., & Friston, K. J. (2000). Voxel-based morphometry--the methods. *Neuroimage, 11*(6 Pt 1), 805-821. Retrieved from https://www.ncbi.nlm.nih.gov/pubmed/10860804. doi:10.1006/nimg.2000.0582

Backman, J. D., Li, A. H., Marcketta, A., Sun, D., Mbatchou, J., Kessler, M. D., . . . Ferreira, M. A. R. (2021). Exome sequencing and analysis of 454,787 UK Biobank participants. *Nature, 599*(7886), 628-634. Retrieved from https://www.ncbi.nlm.nih.gov/pubmed/34662886. doi:10.1038/s41586-021-04103-z

Backstrom, D., Eriksson Domellof, M., Granasen, G., Linder, J., Mayans, S., Elgh, E., . . . Forsgren, L. (2018). Polymorphisms in dopamine-associated genes and cognitive decline in Parkinson's disease. *Acta Neurol Scand, 137*(1), 91-98. Retrieved from https://www.ncbi.nlm.nih.gov/pubmed/28869277. doi:10.1111/ane.12812

Batalle, D., Munoz-Moreno, E., Figueras, F., Bargallo, N., Eixarch, E., & Gratacos, E. (2013). Normalization of similarity-based individual brain networks from gray matter MRI and its association with neurodevelopment in infants with intrauterine growth restriction. *Neuroimage, 83*, 901-911. Retrieved from https://www.ncbi.nlm.nih.gov/pubmed/23886985. doi:10.1016/j.neuroimage.2013.07.045

Bekris, L. M., Tsuang, D. W., Peskind, E. R., Yu, C. E., Montine, T. J., Zhang, J., . . . Leverenz, J. B. (2015). Cerebrospinal fluid Abeta42 levels and APP processing pathway genes in Parkinson's disease. *Mov Disord, 30*(7), 936-944. Retrieved from https://www.ncbi.nlm.nih.gov/pubmed/25808939. doi:10.1002/mds.26172

Bennett, M. R., Farnell, L., & Gibson, W. G. (2008). Origins of the BOLD changes due to synaptic activity at astrocytes abutting arteriolar smooth muscle. *J Theor Biol, 252*(1), 123-130. Retrieved from https://www.ncbi.nlm.nih.gov/pubmed/18339404. doi:10.1016/j.jtbi.2008.01.022

Bialecka, M., Kurzawski, M., Roszmann, A., Robowski, P., Sitek, E. J., Honczarenko, K., . . . Slawek, J. (2012). Association of COMT, MTHFR, and SLC19A1(RFC-1) polymorphisms with homocysteine blood levels and cognitive impairment in Parkinson's disease. *Pharmacogenet Genomics, 22*(10), 716-724. Retrieved from https://www.ncbi.nlm.nih.gov/pubmed/22890010. doi:10.1097/FPC.0b013e32835693f7

Bingol, B., Tea, J. S., Phu, L., Reichelt, M., Bakalarski, C. E., Song, Q., . . . Sheng, M. (2014). The mitochondrial deubiquitinase USP30 opposes parkin-mediated mitophagy. *Nature, 510*(7505), 370-375. Retrieved from https://www.ncbi.nlm.nih.gov/pubmed/24896179. doi:10.1038/nature13418

Brendza, R., Lin, H., Stark, K., Foreman, O., Tao, J., Pierce, A., . . . Friedman, B. A. (2021). Genetic ablation of Gpnmb does not alter synuclein-related pathology. *Neurobiol Dis, 159*, 105494. Retrieved from https://www.ncbi.nlm.nih.gov/pubmed/34464706. doi:10.1016/j.nbd.2021.105494

Budge, K. M., Neal, M. L., Richardson, J. R., & Safadi, F. F. (2020). Transgenic Overexpression of GPNMB Protects Against MPTP-Induced Neurodegeneration. *Mol Neurobiol, 57*(7), 2920-2933. Retrieved from https://www.ncbi.nlm.nih.gov/pubmed/32436108. doi:10.1007/s12035-020-01921-6

Burmann, B. M., Gerez, J. A., Matecko-Burmann, I., Campioni, S., Kumari, P., Ghosh, D., . . . Hiller, S. (2020). Regulation of alpha-synuclein by chaperones in mammalian cells. *Nature, 577*(7788), 127-132. Retrieved from https://www.ncbi.nlm.nih.gov/pubmed/31802003. doi:10.1038/s41586-019-1808-9

Caspers, J., Rubbert, C., Eickhoff, S. B., Hoffstaedter, F., Sudmeyer, M., Hartmann, C. J., . . . Mathys, C. (2021). Within- and across-network alterations of the sensorimotor network in Parkinson's disease. *Neuroradiology, 63*(12), 2073-2085. Retrieved from https://www.ncbi.nlm.nih.gov/pubmed/34019112. doi:10.1007/s00234-021-02731-w

Chang, D., Nalls, M. A., Hallgrimsdottir, I. B., Hunkapiller, J., van der Brug, M., Cai, F., . . . Graham, R. R. (2017). A meta-analysis of genome-wide association studies identifies 17 new Parkinson's disease risk loci. *Nat Genet, 49*(10), 1511-1516. Retrieved from https://www.ncbi.nlm.nih.gov/pubmed/28892059. doi:10.1038/ng.3955

Chen, C. M., Chen, Y. C., Chiang, M. C., Fung, H. C., Chang, K. H., Lee-Chen, G. J., & Wu, Y. R. (2016). Association of GCH1 and MIR4697, but not SIPA1L2 and VPS13C polymorphisms, with Parkinson's disease in Taiwan. *Neurobiol Aging, 39*, 221 e221-225. Retrieved from https://www.ncbi.nlm.nih.gov/pubmed/26804608. doi:10.1016/j.neurobiolaging.2015.12.016

Cookson, M. R. (2010). The role of leucine-rich repeat kinase 2 (LRRK2) in Parkinson's disease. *Nat Rev Neurosci, 11*(12), 791-797. Retrieved from https://www.ncbi.nlm.nih.gov/pubmed/21088684. doi:10.1038/nrn2935

Corvol, J. C., Bonnet, C., Charbonnier-Beaupel, F., Bonnet, A. M., Fievet, M. H., Bellanger, A., . . . Vidailhet, M. (2011). The COMT Val158Met polymorphism affects the response to entacapone in Parkinson's disease: a randomized crossover clinical trial. *Ann Neurol, 69*(1), 111-118. Retrieved from https://www.ncbi.nlm.nih.gov/pubmed/21280081. doi:10.1002/ana.22155

Coyne, A. N., Baskerville, V., Zaepfel, B. L., Dickson, D. W., Rigo, F., Bennett, F., . . . Rothstein, J. D. (2021). Nuclear accumulation of CHMP7 initiates nuclear pore complex injury and subsequent TDP-43 dysfunction in sporadic and familial ALS. *Sci Transl Med, 13*(604). Retrieved from https://www.ncbi.nlm.nih.gov/pubmed/34321318. doi:10.1126/scitranslmed.abe1923

Coyne, A. N., & Rothstein, J. D. (2022). Nuclear pore complexes - a doorway to neural injury in neurodegeneration. *Nat Rev Neurol, 18*(6), 348-362. Retrieved from https://www.ncbi.nlm.nih.gov/pubmed/35488039. doi:10.1038/s41582-022-00653-6

Coyne, A. N., Zaepfel, B. L., Hayes, L., Fitchman, B., Salzberg, Y., Luo, E. C., . . . Rothstein, J. D. (2020). G4C2 Repeat RNA Initiates a POM121-Mediated Reduction in Specific Nucleoporins in C9orf72 ALS/FTD. *Neuron, 107*(6), 1124-1140 e1111. Retrieved from https://www.ncbi.nlm.nih.gov/pubmed/32673563. doi:10.1016/j.neuron.2020.06.027

Cui, X., Xu, C., Zhang, L., & Wang, Y. (2021). Identification of Parkinson's Disease-Causing Genes via Omics Data. *Front Genet, 12*, 712164. Retrieved from https://www.ncbi.nlm.nih.gov/pubmed/34394198. doi:10.3389/fgene.2021.712164

Dahnke, R., Yotter, R. A., & Gaser, C. (2013). Cortical thickness and central surface estimation. *Neuroimage, 65*, 336-348. Retrieved from https://www.ncbi.nlm.nih.gov/pubmed/23041529. doi:10.1016/j.neuroimage.2012.09.050

Davis, A. A., Andruska, K. M., Benitez, B. A., Racette, B. A., Perlmutter, J. S., & Cruchaga, C. (2016). Variants in GBA, SNCA, and MAPT influence Parkinson disease risk, age at onset, and progression. *Neurobiol Aging, 37*, 209 e201-209 e207. Retrieved from https://www.ncbi.nlm.nih.gov/pubmed/26601739. doi:10.1016/j.neurobiolaging.2015.09.014

Deniston, C. K., Salogiannis, J., Mathea, S., Snead, D. M., Lahiri, I., Matyszewski, M., . . . Leschziner, A. E. (2020). Structure of LRRK2 in Parkinson's disease and model for microtubule interaction. *Nature, 588*(7837), 344-349. Retrieved from https://www.ncbi.nlm.nih.gov/pubmed/32814344. doi:10.1038/s41586-020-2673-2

Diaz-Ortiz, M. E., Seo, Y., Posavi, M., Carceles Cordon, M., Clark, E., Jain, N., . . . Chen-Plotkin, A. S. (2022). GPNMB confers risk for Parkinson's disease through interaction with alpha-synuclein. *Science, 377*(6608), eabk0637. Retrieved from https://www.ncbi.nlm.nih.gov/pubmed/35981040. doi:10.1126/science.abk0637

Dunn, A. R., O'Connell, K. M. S., & Kaczorowski, C. C. (2019). Gene-by-environment interactions in Alzheimer's disease and Parkinson's disease. *Neurosci Biobehav Rev, 103*, 73-80. Retrieved from https://www.ncbi.nlm.nih.gov/pubmed/31207254. doi:10.1016/j.neubiorev.2019.06.018

Fang, J., Chen, H., Cao, Z., Jiang, Y., Ma, L., Ma, H., & Feng, T. (2017). Impaired brain network architecture in newly diagnosed Parkinson's disease based on graph theoretical analysis. *Neurosci Lett, 657*, 151-158. Retrieved from https://www.ncbi.nlm.nih.gov/pubmed/28789983. doi:10.1016/j.neulet.2017.08.002

Farrow, S. L., Schierding, W., Gokuladhas, S., Golovina, E., Fadason, T., Cooper, A. A., & O'Sullivan, J. M. (2022). Establishing gene regulatory networks from Parkinson's disease risk loci. *Brain*. Retrieved from https://www.ncbi.nlm.nih.gov/pubmed/35094046. doi:10.1093/brain/awac022

Filippi, M., Basaia, S., Canu, E., Imperiale, F., Magnani, G., Falautano, M., . . . Agosta, F. (2020). Changes in functional and structural brain connectome along the Alzheimer's disease continuum. *Mol Psychiatry, 25*(1), 230-239. Retrieved from https://www.ncbi.nlm.nih.gov/pubmed/29743583. doi:10.1038/s41380-018-0067-8

Fishman, I., Datko, M., Cabrera, Y., Carper, R. A., & Muller, R. A. (2015). Reduced integration and differentiation of the imitation network in autism: A combined functional connectivity magnetic resonance imaging and diffusion-weighted imaging study. *Ann Neurol, 78*(6), 958-969. Retrieved from https://www.ncbi.nlm.nih.gov/pubmed/26418284. doi:10.1002/ana.24533

Fusco, G., Chen, S. W., Williamson, P. T. F., Cascella, R., Perni, M., Jarvis, J. A., . . . De Simone, A. (2017). Structural basis of membrane disruption and cellular toxicity by alpha-synuclein oligomers. *Science, 358*(6369), 1440-1443. Retrieved from https://www.ncbi.nlm.nih.gov/pubmed/29242346. doi:10.1126/science.aan6160

Glahn, D. C., Thompson, P. M., & Blangero, J. (2007). Neuroimaging endophenotypes: strategies for finding genes influencing brain structure and function. *Hum Brain Mapp, 28*(6), 488-501. Retrieved from https://www.ncbi.nlm.nih.gov/pubmed/17440953. doi:10.1002/hbm.20401

Guo, M., Ren, Y., Yu, H., Yang, H., Cao, C., Li, Y., & Fan, G. (2020). Alterations in Degree Centrality and Functional Connectivity in Parkinson's Disease Patients With Freezing of Gait: A Resting-State Functional Magnetic Resonance Imaging Study. *Front Neurosci, 14*, 582079. Retrieved from https://www.ncbi.nlm.nih.gov/pubmed/33224024. doi:10.3389/fnins.2020.582079

Hernandez, L. M., Krasileva, K., Green, S. A., Sherman, L. E., Ponting, C., McCarron, R., . . . Dapretto, M. (2017). Additive effects of oxytocin receptor gene polymorphisms on reward circuitry in youth with autism. *Mol Psychiatry, 22*(8), 1134-1139. Retrieved from https://www.ncbi.nlm.nih.gov/pubmed/27843152. doi:10.1038/mp.2016.209

Hong, S. J., Bernhardt, B. C., Gill, R. S., Bernasconi, N., & Bernasconi, A. (2017). The spectrum of structural and functional network alterations in malformations of cortical development. *Brain, 140*(8), 2133-2143. Retrieved from https://www.ncbi.nlm.nih.gov/pubmed/28899007. doi:10.1093/brain/awx145

Imperiale, F., Agosta, F., Canu, E., Markovic, V., Inuggi, A., Jecmenica-Lukic, M., . . . Filippi, M. (2018). Brain structural and functional signatures of impulsive-compulsive behaviours in Parkinson's disease. *Mol Psychiatry, 23*(2), 459-466. Retrieved from https://www.ncbi.nlm.nih.gov/pubmed/28265121. doi:10.1038/mp.2017.18

International Parkinson Disease Genomics, C., Nalls, M. A., Plagnol, V., Hernandez, D. G., Sharma, M., Sheerin, U. M., . . . Wood, N. W. (2011). Imputation of sequence variants for identification of genetic risks for Parkinson's disease: a meta-analysis of genome-wide association studies. *Lancet, 377*(9766), 641-649. Retrieved from https://www.ncbi.nlm.nih.gov/pubmed/21292315. doi:10.1016/S0140-6736(10)62345-8

Jessen, S. B., Brazhe, A., Lind, B. L., Mathiesen, C., Thomsen, K., Jensen, K., & Lauritzen, M. (2015). GABAA Receptor-Mediated Bidirectional Control of Synaptic Activity, Intracellular Ca2+, Cerebral Blood Flow, and Oxygen Consumption in Mouse Somatosensory Cortex In Vivo. *Cereb Cortex, 25*(9), 2594-2609. Retrieved from https://www.ncbi.nlm.nih.gov/pubmed/24692513. doi:10.1093/cercor/bhu058

Ji, G. J., Ren, C., Li, Y., Sun, J., Liu, T., Gao, Y., . . . Wang, K. (2019). Regional and network properties of white matter function in Parkinson's disease. *Hum Brain Mapp, 40*(4), 1253-1263. Retrieved from https://www.ncbi.nlm.nih.gov/pubmed/30414340. doi:10.1002/hbm.24444

Jiang, Z., Huang, Y., Zhang, P., Han, C., Lu, Y., Mo, Z., . . . Ling, F. (2020). Characterization of a pathogenic variant in GBA for Parkinson's disease with mild cognitive impairment patients. *Mol Brain, 13*(1), 102. Retrieved from https://www.ncbi.nlm.nih.gov/pubmed/32641146. doi:10.1186/s13041-020-00637-x

Kahali, S., Raichle, M. E., & Yablonskiy, D. A. (2021). The Role of the Human Brain Neuron-Glia-Synapse Composition in Forming Resting-State Functional Connectivity Networks. *Brain Sci, 11*(12). Retrieved from https://www.ncbi.nlm.nih.gov/pubmed/34942867. doi:10.3390/brainsci11121565

Khera, A. V., Chaffin, M., Aragam, K. G., Haas, M. E., Roselli, C., Choi, S. H., . . . Kathiresan, S. (2018). Genome-wide polygenic scores for common diseases identify individuals with risk equivalent to monogenic mutations. *Nat Genet, 50*(9), 1219-1224. Retrieved from https://www.ncbi.nlm.nih.gov/pubmed/30104762. doi:10.1038/s41588-018-0183-z

Latora, V., & Marchiori, M. (2001). Efficient behavior of small-world networks. *Phys Rev Lett, 87*(19), 198701. Retrieved from https://www.ncbi.nlm.nih.gov/pubmed/11690461. doi:10.1103/PhysRevLett.87.198701

Latourelle, J. C., Beste, M. T., Hadzi, T. C., Miller, R. E., Oppenheim, J. N., Valko, M. P., . . . Venuto, C. S. (2017). Large-scale identification of clinical and genetic predictors of motor progression in patients with newly diagnosed Parkinson's disease: a longitudinal cohort study and validation. *Lancet Neurol, 16*(11), 908-916. Retrieved from https://www.ncbi.nlm.nih.gov/pubmed/28958801. doi:10.1016/S1474-4422(17)30328-9

Li, R., Chen, Y., Ritchie, M. D., & Moore, J. H. (2020). Electronic health records and polygenic risk scores for predicting disease risk. *Nat Rev Genet, 21*(8), 493-502. Retrieved from https://www.ncbi.nlm.nih.gov/pubmed/32235907. doi:10.1038/s41576-020-0224-1

Li, Y. O., Adali, T., & Calhoun, V. D. (2007). Estimating the number of independent components for functional magnetic resonance imaging data. *Hum Brain Mapp, 28*(11), 1251-1266. Retrieved from https://www.ncbi.nlm.nih.gov/pubmed/17274023. doi:10.1002/hbm.20359

Liu, S. Y., Wile, D. J., Fu, J. F., Valerio, J., Shahinfard, E., McCormick, S., . . . Stoessl, A. J. (2018). The effect of LRRK2 mutations on the cholinergic system in manifest and

premanifest stages of Parkinson's disease: a cross-sectional PET study. *Lancet Neurol, 17*(4), 309-316. Retrieved from https://www.ncbi.nlm.nih.gov/pubmed/29456161. doi:10.1016/S1474-4422(18)30032-2

Luo, C. Y., Guo, X. Y., Song, W., Chen, Q., Cao, B., Yang, J., . . . Shang, H. F. (2015). Functional connectome assessed using graph theory in drug-naive Parkinson's disease. *J Neurol, 262*(6), 1557-1567. Retrieved from https://www.ncbi.nlm.nih.gov/pubmed/25929663. doi:10.1007/s00415-015-7750-3

Manzanillo, P. S., Ayres, J. S., Watson, R. O., Collins, A. C., Souza, G., Rae, C. S., . . . Cox, J. S. (2013). The ubiquitin ligase parkin mediates resistance to intracellular pathogens. *Nature, 501*(7468), 512-516. Retrieved from https://www.ncbi.nlm.nih.gov/pubmed/24005326. doi:10.1038/nature12566

Marek, K., Chowdhury, S., Siderowf, A., Lasch, S., Coffey, C. S., Caspell-Garcia, C., . . . Parkinson's Progression Markers, I. (2018). The Parkinson's progression markers initiative (PPMI) - establishing a PD biomarker cohort. *Ann Clin Transl Neurol, 5*(12), 1460-1477. Retrieved from https://www.ncbi.nlm.nih.gov/pubmed/30564614. doi:10.1002/acn3.644

Mascheretti, S., De Luca, A., Trezzi, V., Peruzzo, D., Nordio, A., Marino, C., & Arrigoni, F. (2017). Neurogenetics of developmental dyslexia: from genes to behavior through brain neuroimaging and cognitive and sensorial mechanisms. *Transl Psychiatry, 7*(1), e987. Retrieved from https://www.ncbi.nlm.nih.gov/pubmed/28045463. doi:10.1038/tp.2016.240

Mata, I. F., Leverenz, J. B., Weintraub, D., Trojanowski, J. Q., Hurtig, H. I., Van Deerlin, V. M., . . . Zabetian, C. P. (2014). APOE, MAPT, and SNCA genes and cognitive performance in Parkinson disease. *JAMA Neurol, 71*(11), 1405-1412. Retrieved from https://www.ncbi.nlm.nih.gov/pubmed/25178429. doi:10.1001/jamaneurol.2014.1455

Matheoud, D., Cannon, T., Voisin, A., Penttinen, A. M., Ramet, L., Fahmy, A. M., . . . Desjardins, M. (2019). Intestinal infection triggers Parkinson's disease-like symptoms in Pink1(-/-) mice. *Nature, 571*(7766), 565-569. Retrieved from https://www.ncbi.nlm.nih.gov/pubmed/31316206. doi:10.1038/s41586-019-1405-y

Matheoud, D., Sugiura, A., Bellemare-Pelletier, A., Laplante, A., Rondeau, C., Chemali, M., . . . Desjardins, M. (2016). Parkinson's Disease-Related Proteins PINK1 and Parkin Repress Mitochondrial Antigen Presentation. *Cell, 166*(2), 314-327. Retrieved from https://www.ncbi.nlm.nih.gov/pubmed/27345367. doi:10.1016/j.cell.2016.05.039

Moloney, E. B., Moskites, A., Ferrari, E. J., Isacson, O., & Hallett, P. J. (2018). The glycoprotein GPNMB is selectively elevated in the substantia nigra of Parkinson's disease patients and increases after lysosomal stress. *Neurobiol Dis, 120*, 1-11. Retrieved from https://www.ncbi.nlm.nih.gov/pubmed/30149180. doi:10.1016/j.nbd.2018.08.013

Murthy, M. N., Blauwendraat, C., Ukbec, Guelfi, S., Ipdgc, Hardy, J., . . . Trabzuni, D. (2017). Increased brain expression of GPNMB is associated with genome wide significant risk for Parkinson's disease on chromosome 7p15.3. *Neurogenetics, 18*(3), 121-133. Retrieved from https://www.ncbi.nlm.nih.gov/pubmed/28391543. doi:10.1007/s10048-017-0514-8

Nalls, M. A., Blauwendraat, C., Vallerga, C. L., Heilbron, K., Bandres-Ciga, S., Chang, D., . . . International Parkinson's Disease Genomics, C. (2019). Identification of novel risk loci, causal insights, and heritable risk for Parkinson's disease: a meta-analysis of genome-wide association studies. *Lancet Neurol, 18*(12), 1091-1102. Retrieved from https://www.ncbi.nlm.nih.gov/pubmed/31701892. doi:10.1016/S1474-4422(19)30320-5

Neal, M. L., Boyle, A. M., Budge, K. M., Safadi, F. F., & Richardson, J. R. (2018). The glycoprotein GPNMB attenuates astrocyte inflammatory responses through the CD44 receptor. *J Neuroinflammation, 15*(1), 73. Retrieved from https://www.ncbi.nlm.nih.gov/pubmed/29519253. doi:10.1186/s12974-018-1100-1

Nguyen, H. N., Byers, B., Cord, B., Shcheglovitov, A., Byrne, J., Gujar, P., . . . Pera, R. R. (2011). LRRK2 mutant iPSC-derived DA neurons demonstrate increased susceptibility to oxidative stress. *Cell Stem Cell, 8*(3), 267-280. Retrieved from https://www.ncbi.nlm.nih.gov/pubmed/21362567. doi:10.1016/j.stem.2011.01.013

Nishioka, K., Hayashi, S., Farrer, M. J., Singleton, A. B., Yoshino, H., Imai, H., . . . Hattori, N. (2006). Clinical heterogeneity of alpha-synuclein gene duplication in Parkinson's disease. *Ann Neurol, 59*(2), 298-309. Retrieved from https://www.ncbi.nlm.nih.gov/pubmed/16358335. doi:10.1002/ana.20753

Parkinson Progression Marker, I. (2011). The Parkinson Progression Marker Initiative (PPMI). *Prog Neurobiol, 95*(4), 629-635. Retrieved from https://www.ncbi.nlm.nih.gov/pubmed/21930184. doi:10.1016/j.pneurobio.2011.09.005

Peng, C., Gathagan, R. J., Covell, D. J., Medellin, C., Stieber, A., Robinson, J. L., . . . Lee, V. M. (2018). Cellular milieu imparts distinct pathological alpha-synuclein strains in alpha-synucleinopathies. *Nature, 557*(7706), 558-563. Retrieved from https://www.ncbi.nlm.nih.gov/pubmed/29743672. doi:10.1038/s41586-018-0104-4

Pierce, S., & Coetzee, G. A. (2017). Parkinson's disease-associated genetic variation is linked to quantitative expression of inflammatory genes. *PLoS One, 12*(4), e0175882. Retrieved from https://www.ncbi.nlm.nih.gov/pubmed/28407015. doi:10.1371/journal.pone.0175882

Robinet, P., Ritchey, B., Lorkowski, S. W., Alzayed, A. M., DeGeorgia, S., Schodowski, E., . . . Smith, J. D. (2021). Quantitative trait locus mapping identifies the Gpnmb gene as a modifier of mouse macrophage lysosome function. *Sci Rep, 11*(1), 10249. Retrieved from https://www.ncbi.nlm.nih.gov/pubmed/33986446. doi:10.1038/s41598-021-89800-5

Rubinov, M., & Sporns, O. (2010). Complex network measures of brain connectivity: uses and interpretations. *Neuroimage, 52*(3), 1059-1069. Retrieved from https://www.ncbi.nlm.nih.gov/pubmed/19819337. doi:10.1016/j.neuroimage.2009.10.003

Satake, W., Nakabayashi, Y., Mizuta, I., Hirota, Y., Ito, C., Kubo, M., . . . Toda, T. (2009). Genome-wide association study identifies common variants at four loci as genetic risk factors for Parkinson's disease. *Nat Genet, 41*(12), 1303-1307. Retrieved from https://www.ncbi.nlm.nih.gov/pubmed/19915576. doi:10.1038/ng.485

Shahnawaz, M., Mukherjee, A., Pritzkow, S., Mendez, N., Rabadia, P., Liu, X., . . . Soto, C. (2020). Discriminating alpha-synuclein strains in Parkinson's disease and multiple system atrophy. *Nature, 578*(7794), 273-277. Retrieved from https://www.ncbi.nlm.nih.gov/pubmed/32025029. doi:10.1038/s41586-020-1984-7

Simuni, T., Uribe, L., Cho, H. R., Caspell-Garcia, C., Coffey, C. S., Siderowf, A., . . . Investigators, P. (2020). Clinical and dopamine transporter imaging characteristics of non-manifest LRRK2 and GBA mutation carriers in the Parkinson's Progression Markers Initiative (PPMI): a cross-sectional study. *Lancet Neurol, 19*(1), 71-80. Retrieved from https://www.ncbi.nlm.nih.gov/pubmed/31678032. doi:10.1016/S1474-4422(19)30319-9

Sliter, D. A., Martinez, J., Hao, L., Chen, X., Sun, N., Fischer, T. D., . . . Youle, R. J. (2018). Parkin and PINK1 mitigate STING-induced inflammation. *Nature, 561*(7722), 258-

262. Retrieved from https://www.ncbi.nlm.nih.gov/pubmed/30135585. doi:10.1038/s41586-018-0448-9

Tang, C., Wang, W., Shi, M., Zhang, N., Zhou, X., Li, X., . . . Gao, D. (2019). Meta-Analysis of the Effects of the Catechol-O-Methyltransferase Val158/108Met Polymorphism on Parkinson's Disease Susceptibility and Cognitive Dysfunction. *Front Genet, 10*, 644. Retrieved from https://www.ncbi.nlm.nih.gov/pubmed/31354790. doi:10.3389/fgene.2019.00644

Tijms, B. M., Series, P., Willshaw, D. J., & Lawrie, S. M. (2012). Similarity-based extraction of individual networks from gray matter MRI scans. *Cereb Cortex, 22*(7), 1530-1541. Retrieved from https://www.ncbi.nlm.nih.gov/pubmed/21878484. doi:10.1093/cercor/bhr221

van Veen, S., Martin, S., Van den Haute, C., Benoy, V., Lyons, J., Vanhoutte, R., . . . Vangheluwe, P. (2020). ATP13A2 deficiency disrupts lysosomal polyamine export. *Nature, 578*(7795), 419-424. Retrieved from https://www.ncbi.nlm.nih.gov/pubmed/31996848. doi:10.1038/s41586-020-1968-7

Vuckovic, D., Bao, E. L., Akbari, P., Lareau, C. A., Mousas, A., Jiang, T., . . . Soranzo, N. (2020). The Polygenic and Monogenic Basis of Blood Traits and Diseases. *Cell, 182*(5), 1214-1231 e1211. Retrieved from https://www.ncbi.nlm.nih.gov/pubmed/32888494. doi:10.1016/j.cell.2020.08.008

Wang, J. H., Zuo, X. N., Gohel, S., Milham, M. P., Biswal, B. B., & He, Y. (2011). Graph theoretical analysis of functional brain networks: test-retest evaluation on short- and long-term resting-state functional MRI data. *PLoS One, 6*(7), e21976. Retrieved from https://www.ncbi.nlm.nih.gov/pubmed/21818285. doi:10.1371/journal.pone.0021976

Watanabe, R., Buschauer, R., Bohning, J., Audagnotto, M., Lasker, K., Lu, T. W., . . . Villa, E. (2020). The In Situ Structure of Parkinson's Disease-Linked LRRK2. *Cell, 182*(6), 1508-1518 e1516. Retrieved from https://www.ncbi.nlm.nih.gov/pubmed/32783917. doi:10.1016/j.cell.2020.08.004

Webb, J., & Willette, A. A. (2017). Aging modifies the effect of GCH1 RS11158026 on DAT uptake and Parkinson's disease clinical severity. *Neurobiol Aging, 50*, 39-46. Retrieved from https://www.ncbi.nlm.nih.gov/pubmed/27871051. doi:10.1016/j.neurobiolaging.2016.10.006

Wei, L., Zhang, J., Long, Z., Wu, G. R., Hu, X., Zhang, Y., & Wang, J. (2014). Reduced topological efficiency in cortical-basal Ganglia motor network of Parkinson's disease: a resting state fMRI study. *PLoS One, 9*(10), e108124. Retrieved from https://www.ncbi.nlm.nih.gov/pubmed/25279557. doi:10.1371/journal.pone.0108124

White, J. D., Indencleef, K., Naqvi, S., Eller, R. J., Hoskens, H., Roosenboom, J., . . . Claes, P. (2021). Insights into the genetic architecture of the human face. *Nat Genet, 53*(1), 45-53. Retrieved from https://www.ncbi.nlm.nih.gov/pubmed/33288918. doi:10.1038/s41588-020-00741-7

Wie, J., Liu, Z., Song, H., Tropea, T. F., Yang, L., Wang, H., . . . Ren, D. (2021). A growth-factor-activated lysosomal K(+) channel regulates Parkinson's pathology. *Nature*. Retrieved from https://www.ncbi.nlm.nih.gov/pubmed/33505021. doi:10.1038/s41586-021-03185-z

Xu, X., Luo, S., Wen, X., Wang, X., Yin, J., Luo, X., . . . Ma, G. (2021). Genetic Contribution of Synapse-Associated Protein 97 to Orbitofrontal-Striatal-Thalamic Circuitry Connectivity Changes in First-Episode Schizophrenia. *Front Psychiatry, 12*, 691007. Retrieved from https://www.ncbi.nlm.nih.gov/pubmed/34349683. doi:10.3389/fpsyt.2021.691007

Zalesky, A., Fornito, A., & Bullmore, E. T. (2010). Network-based statistic: identifying differences in brain networks. *Neuroimage, 53*(4), 1197-1207. Retrieved from

https://www.ncbi.nlm.nih.gov/pubmed/20600983. doi:10.1016/j.neuroimage.2010.06.041

Zhang, D., Wang, J., Liu, X., Chen, J., & Liu, B. (2015). Aberrant Brain Network Efficiency in Parkinson's Disease Patients with Tremor: A Multi-Modality Study. *Front Aging Neurosci, 7*, 169. Retrieved from https://www.ncbi.nlm.nih.gov/pubmed/26379547. doi:10.3389/fnagi.2015.00169

Zhang, K., Daigle, J. G., Cunningham, K. M., Coyne, A. N., Ruan, K., Grima, J. C., . . . Lloyd, T. E. (2018). Stress Granule Assembly Disrupts Nucleocytoplasmic Transport. *Cell, 173*(4), 958-971 e917. Retrieved from https://www.ncbi.nlm.nih.gov/pubmed/29628143. doi:10.1016/j.cell.2018.03.025

Zhao, B., Li, T., Smith, S. M., Xiong, D., Wang, X., Yang, Y., . . . Zhu, H. (2022). Common variants contribute to intrinsic human brain functional networks. *Nat Genet, 54*(4), 508-517. Retrieved from https://www.ncbi.nlm.nih.gov/pubmed/35393594. doi:10.1038/s41588-022-01039-6